PHYSICAL REVIEW B VOLUME 56, NUMBER 11 15 SEPTEMBER 1997-I

Selective ion-channeling study of misfit dislocation grids in semiconductor heterostructures: Theory and experiments

M. Mazzer,* A. V. Drigo, and F. Romanato
INFM at the Department of Physics, University of Padova, Via F. Marzolo, 8-35131 Padova, Italy

G. Salviati and L. Lazzarini
MASPEC Institute, CNR, Via Chiavari, 18/a-43100 Parma, Italy
(Received 7 August 1996)

Planar dechanneling by networks of misfit dislocations was measured in a series of $In_xGa_{1-x}As/GaAs$ samples (001) grown by molecular-beam epitaxy. At the beginning of the strain-relaxation process the dechanneling probability exhibits different values for nominally equivalent (110) planes. At larger strain relaxation, the dechanneling probability saturates at a value around $\frac{1}{2}$ as the beam-energy increases. In order to explain these results a new model for planar dechanneling by dislocations is proposed. This model is based on the harmonic approximation of the continuum potential but anharmonicity effects are taken into account. The perturbation to the harmonic oscillations caused by the lattice plane curvature around a dislocation is written in terms of a distortion function that depends only on the geometrical configuration of the channeling direction and of the dislocation line. This function is explicitly calculated for geometrical configurations relevant to the present samples allowing us then to solve the equation of motion. The results show that the dechanneling probability saturates at a level sensibly lower than 100% due to the quasiplanar distribution of dislocations. Without any adjustable parameter, the comparison between computed and measured dechanneling probabilities supplies dislocation density values in excellent agreement with those measured by transmission electron microscopy and in good agreement with results deduced from previous strain-relaxation data. [S0163-1829(97)00235-X]

I. INTRODUCTION

It is well known that ion channeling is a valuable tool in surface science. Beside clean surface structure, it can be applied to characterize structure and crystal quality of surface layers together with their interface.[1] In particular, in the last decade the ion-channeling technique has been applied to the study of strained epitaxial layers. Since the early work[2] demonstrating the ability of ion channeling to measure the tetragonal distortion of mismatched heterostructures, the technique has now reached a high degree of reliability and precision.[3] It is also well established that ion channeling is sensitive to lattice defects and that their concentration profiles can be easily measured by comparing the Rutherford backscattering spectrometry (RBS) channeling spectrum of the damaged crystal to the corresponding one of a virgin sample. In this view it appears surprising that this technique has not been systematically applied to the study of the misfit dislocations (MD's) appearing at the epilayer-substrate interface once the critical thickness for coherent growth is overcome.[4,5]

Since the pioneering work by Quéré[6] many improvements in the model of the dechanneling by dislocations have been realized.[7–11] However, in any of these models it is very difficult to properly account for the lattice distortion field around a dislocation in a general way, i.e., for an arbitrary orientation of the channeling direction, the dislocation line, and its Burgers vector.

In this paper we develop an analytical model of planar dechanneling based on the harmonic approximation to the continuum planar potential although anharmonicity effects are taken into account in order to better describe the dynamics of the dechanneling process. As usual, the simple harmonic oscillator equation is modified by introducing an ''external force'' term to take into account the perturbation caused by the curvature induced in the lattice planes surrounding the dislocation line. The main point is that the perturbation term can be written as the product of a ''physical'' factor (containing the beam energy, the planar potential, the modulus of the Burgers vector, and the impact parameter of the ion trajectory to the dislocation line) and of a ''geometrical'' factor, which we call ''distortion function.'' Apart from a weak dependence on the material through the Poisson ratio ν, this function depends only on the geometry of the channeling direction and of the dislocation and can be calculated for any given geometrical configuration allowing the solutions to be generalized. The solution of the equation of motion correlates the distribution of the oscillator amplitudes beyond the distortion field to the corresponding distribution of initial dynamical states. This is all that is needed to compute the backscattering probability. For a given geometrical configuration the dechanneling probability is shown to depend on the product of the dislocation density and of the square root of the beam energy.

Although this model of planar dechanneling by dislocations is of general validity, in this paper the solutions are explicitly computed for the 60° MD arrays that are typically found in (001)-grown semiconductor heterostructures like the samples investigated in this work. The main result is that in the case of quasiplanar MD distributions at the interface, the dechanneling probability for sufficiently high beam energies (dislocation densities) saturates at a value around 0.5–0.6, the same value that is experimentally found. This is

 © 1997 The American Physical Society

TABLE I. Description of the $In_xGa_{1-x}As/GaAs$ samples with their dislocation density in the [110] ($N_>$) and [$1\bar{1}0$] ($N_<$) direction in the interface as determined by TEM, dechanneling measurements, and strain relaxation.

			TEM		Dechanneling		Strain[a]	
Sample	x	Thickness (nm)	$N_>$	$N_<$	$N_>$ (10^4 cm^{-1})	$N_<$	$N_>$	$N_<$
1	0.085	310			12.0±1.4	12.0±1.4	15.5±3.0	15.5±3.0
2	0.105	68	4.5±0.9	1.6±0.5	5.1±0.4	0.5±0.3	5.0±4.6	2.0±4.6
3	0.080	200	8.1±0.9	5.4±0.8	8.2±0.4	4.4±0.3	9.5±3.4	7.5±3.4
4	0.150	345			30.0±6.2	30.0±6.2	37.0±3.5	37.0±3.5
5	0.080	810			14.4±1.1	14.4±1.1	19.0±3.0	19.0±3.0

[a]From the data of Refs. 12 and 28.

related to the planar distribution of the dislocations. Moreover, the model shows that dechanneling is sensitive to the dislocation orientation and suggests the way to measure their density in different directions.

Starting from the experimental values of the dechanneling probability this model, which does not contain any adjustable parameter, enables us to calculate the dislocation density (densities). The results are shown to be in excellent agreement with those derived from transmission electron microscopy (TEM) measurements and from previous strain-release data.[12]

II. EXPERIMENT

$In_xGa_{1-x}As$ layers were grown on (001)GaAs substrates in a VG-80 H twin chamber system with continuous substrate rotation at the CSELT laboratory in Torino. Layers were all grown at the substrate temperature of 530 °C under an As pressure of 3×10^{-5} mBar and a V/III equivalent pressure of 50:1. For further details see Ref. 12. The In molar fraction of the samples used in this experiment ranges from 0.08 to 0.15 while the epilayer thickness spans from 68 to 810 nm as shown in Table I.

Samples for TEM analyses were thinned both in plan and in the (110) cross-section geometry by standard mechanochemical procedures followed by low-temperature Ar ion milling. Thinned specimens were examined in a JEOL 2000FX transmission electron microscope working at 200 kV (Scherzer resolution ~0.31 nm) using conventional bright-field or dark-field diffraction contrast imaging and bright-field, axial illumination [110] lattice imaging.

RBS analyses were performed at the Laboratori Nazionali di Legnaro (Padova, Italy) by using $^4He^+$ beams delivered by the 2-MV AN 2000 and the 7-MV CN accelerators. The beam energy was varied from 0.5 to 6 MeV. Channeling spectra were obtained by using a high-precision three-axis goniometer, which allows us to perform also strain measurements.[3] In order to avoid radiation damage accumulation, the beam spot position was moved on the sample surface by means of two translation axes while keeping the beam at the intersection of the rotation axes.

Since the dechanneling information comes from the aligned spectrum normalized to the random one, care was taken in order to avoid any channeling effect in the latter. To this purpose, the random spectra were collected while the sample was tilted 5° from the channeling axis and azimuthally rotated in steps of 0.5° between two principal symmetry planes. The total charge of each spectrum was obtained by integration of the beam current in the isolated scattering chamber acting as a Faraday cup. The accuracy is better than 1%.

III. RESULTS

It is well known that the growth of III-V semiconductor lattice mismatched epitaxial layers with thickness larger than the critical one[4,5] results in the generation of MD grids leading to strain relaxation. In (001)-oriented specimens MD's are arranged in perpendicular arrays aligned along the two ⟨110⟩-type directions in the (001) interface. Due to the absence of inversion symmetry in the zinc-blende lattice, a difference in the dislocation density along the two ⟨110⟩-type directions is expected.[13] Our TEM investigations confirm this general behavior, as shown, for instance, in the two examples of Fig. 1, which are representative of the investigated specimens. Both of the samples in Fig. 1 have an epilayer thickness well above the critical one but they differ in the amount of strain release. Sample 2 [Fig. 1(a)] exhibits a

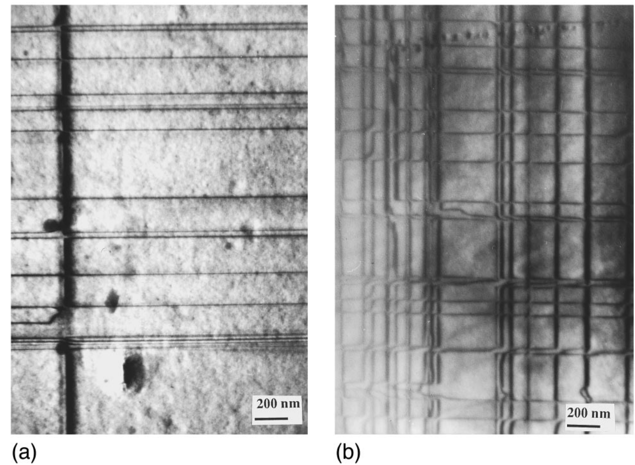

FIG. 1. (001) plan view bright-field zone axis TEM micrographs of two $In_xGa_{1-x}As/GaAs$ layers showing the different MD densities along the two ⟨110⟩-type directions: (a) sample 2, $x=0.105$, $t=68$ nm; (b) sample 3, $x=0.080$, $t=200$ nm. It is worth noting that the dislocations tend to align in bands even at low density.

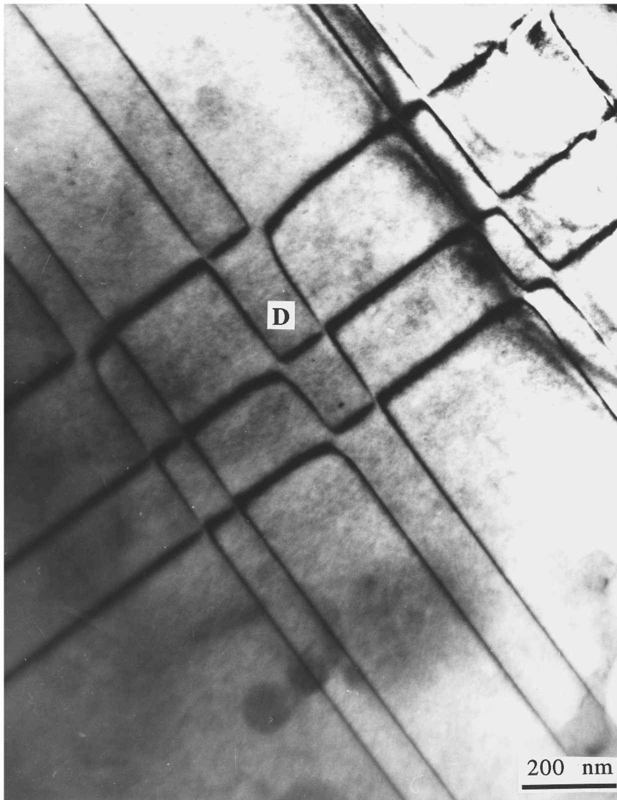

FIG. 2. (001) plan view bright-field zone axis TEM micrograph of a different area of the same specimen of Fig. 1(a). Dipoles (D) resulting from the interaction between two orthogonal dislocations of opposite Burgers vectors are shown.

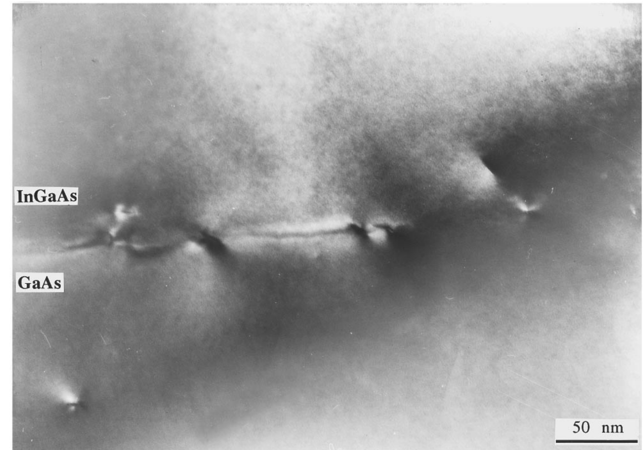

FIG. 3. (110)-oriented cross-section micrograph of sample 5 showing that the MD's are confined within less than 50 nm of the heterointerface.

strain relaxation nearly not measurable (at the limit of the error bar) while for sample 3 [Fig. 1(b)] the 10% of the initial strain (misfit) has been relaxed. It is worth noting that even at low dislocation density [Fig. 1(a)] some dislocations are aligned in bands. This observation will play a non-negligible role in the comparison between the estimate of the average dislocation density as obtained by the dechanneling technique and by the strain relaxation (see Sec. V). Of course, the dislocation density increases with increasing strain relaxation [Fig. 1(b)]. As a consequence, the asymmetry between the two dislocation arrays becomes less marked and eventually disappears as already found by other authors.[14]

Standard $\mathbf{g}\cdot\mathbf{b}$ extinction contrast TEM analyses have confirmed the general observation that MD's were mostly of 60° type as is usually reported for low misfit heterostructures.[15] The $\mathbf{g}\cdot\mathbf{b}$ criterion does not permit us to determine the Burgers vector sign, which in turn determines whether the dislocation relaxes strain or not. The sign determination would require more accurate and complicated procedures; however, it is possible to evidence it by studying the dislocation interactions[16] in TEM micrographs. Among the different types of interaction, some involve dislocations having antiparallel Burgers vectors[17] such as, for instance, the dipoles shown in Fig. 2. The presence of MD's having antiparallel Burgers vectors suggests that not all the misfit lines are effective in releasing the strain, due to the fact that one of these vectors must have the ''wrong'' sign for the strain release.

Another important point to be considered in lattice mismatched heterostructures is the determination of the MD depth location. In principle, MD's can propagate into the buffer and/or substrate layers, they can move at the interface plane, or they can thread through the epilayer. In all the investigated samples, the great majority of the misfit dislocations are arranged just in the plane of the interface as shown, for instance, in Fig. 3. In a few cases dislocations were observed to depart from this planar distribution, in any case being confined within a shallow depth near the interface.

Figure 4 reports the 3-MeV RBS {110} planar and [001] channeling spectra of sample 1 together with the random spectrum and the corresponding GaAs channeling spectra for comparison. The near surface channeling yields for sample 1 and for GaAs are comparable, indicating a nearly perfect surface structure. The presence of dislocations is evidenced by the yield increase in the near-interface region. The com-

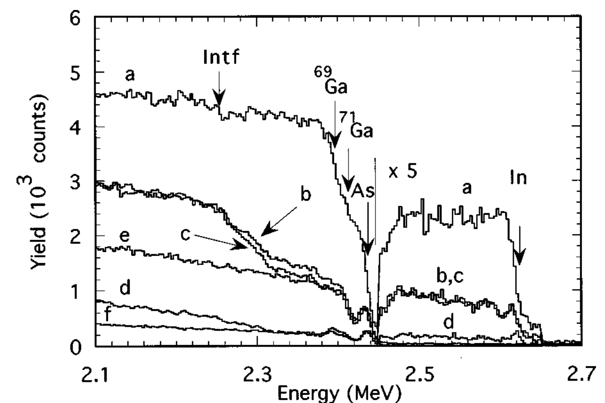

FIG. 4. 3.0-MeV He RBS spectra of sample 1 and of a GaAs substrate as a reference. The arrows indicate the surface scattering energies from different elements or isotopes and the position of the interface (intf). The In signal region of the spectra is multiplied by a factor 5 in order to better show the differences between the spectra. Spectra indicated with the letters from a to d refer to sample 1 and correspond in that order to the random, (110), (1$\overline{1}$0), and [001] directions. Spectra e and f refer to the GaAs sample and correspond, respectively, to the (110) and [001] directions.

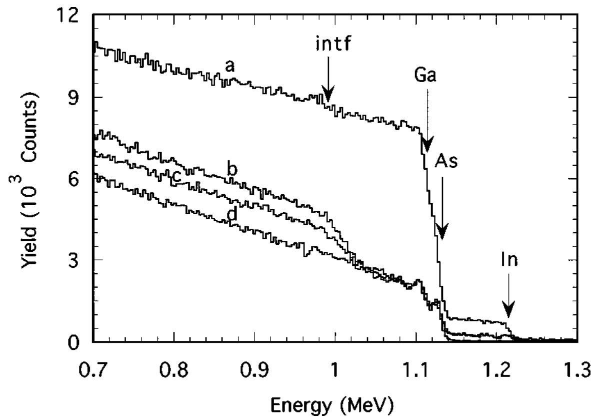

FIG. 5. 1.4-MeV He RBS spectra of sample 3 and of a GaAs substrate as a reference. The arrows indicate the surface scattering energies from different elements and the position of the interface (intf). Spectra a, b, and c refer to sample 3 and correspond in that order to random, (110), and $(1\bar{1}0)$ incidence; spectrum d GaAs {110} planar channeling.

parison between the planar and the axial channeling spectra makes it clear that the dislocation contribution to the dechanneling is more pronounced in the planar than in the axial case. For this reason, and because of the geometry of (110) and $(1\bar{1}0)$ planes, which are either parallel or perpendicular to the dislocation lines, in the following we will be concerned only with planar channeling along these directions.

The high mass resolution achieved at 3 MeV, as shown by the edges of the random spectrum, which are well separated even for the Ga isotopes, complicates the energy-to-depth conversion. As a consequence, in order to extract the depth profile of the dislocations and the dechanneling probability P_d a proper spectrum simulation procedure was used. The details on the simulation and on how the dechanneling probability is obtained from the measured RBS spectra is described in Ref. 18.

From the analysis of the planar spectra in Fig. 4 it turns out that $P_d = 0.55$ and that the defects must be distributed within a maximum depth range from the interface of the order of the experimental depth resolution of the technique (~50 nm), in full agreement with the TEM results. It is worth noting that the yields of the planar channeling spectra do not reach the random yield despite the fact that the ion-beam energy is high. This point, which is most relevant for the remainder of this paper, will be discussed further later. Finally, it is evident that the two {110} spectra in Fig. 4 are nearly indistinguishable, i.e., the dechanneling probability in this case does not depend on the particular orientation of the channeling plane.

A different behavior appears for sample 3, where the yields of the two {110} channeling spectra are significantly different, as shown in Fig. 5. This fact can be explained by the asymmetry in the dislocation distribution shown by the TEM analysis of Fig. 1(b). This fact confirms the previous suggestion that (110) and $(1\bar{1}0)$ channeling planes are particularly suitable for the characterization of MD arrays.

As a first approximation the dechanneling probability P_d is proportional to the dislocation density through the so-called dechanneling factor.[1] The aim of Sec. IV is to discover the quantitative correlation between P_d (the outcome of the experiment) and the dislocation density by developing an original dechanneling model. In order to test this model, the channeling results will be compared to the TEM observations. Since the typical dimensions of the ion-beam spot are orders of magnitude higher than the usually investigated TEM areas, large TEM micrograph maps (~100 μm^2) have been performed on some samples as shown in Fig. 6 for sample 3. These investigations show that the MD arrangement is homogeneous at this scale. The homogeneity of the MD distribution on a larger scale has been also assessed by double crystal x-ray topography on the whole specimen, confirming the reliability of the TEM maps. The MD densities of the two arrays have been obtained directly by counting the number of dislocation lines. The results are reported in Table I as average linear dislocation density. The relative errors have been taken as $1/\sqrt{n}$, n being the number of counted dislocations. A certain number of different interaction types was found and, as an example, Fig. 6 gives an idea of the number and of the distribution of the interactions between the dislocation lines.

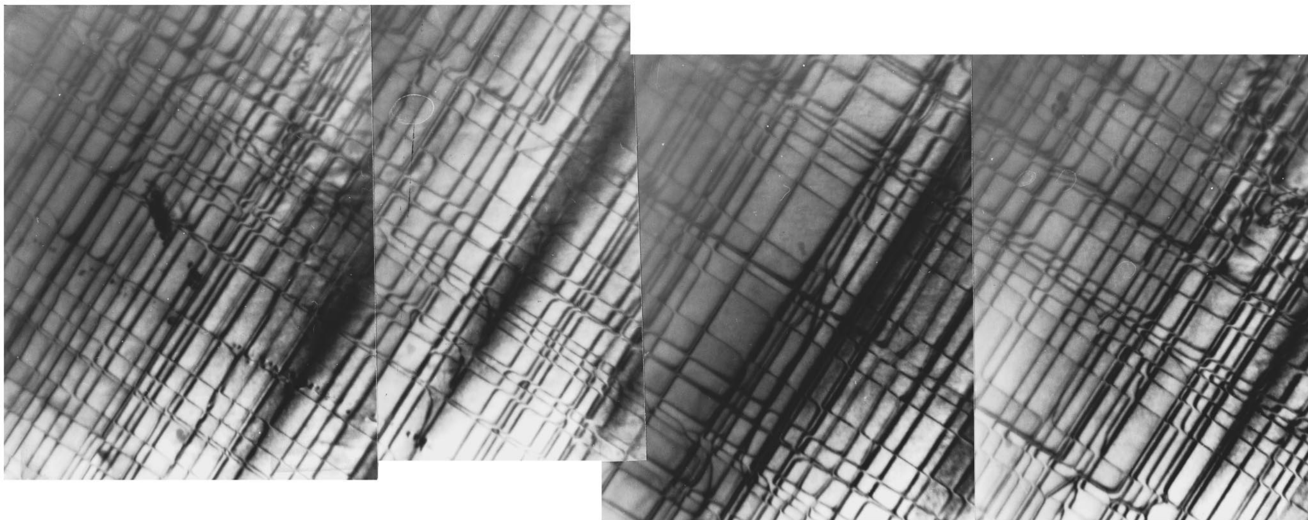

FIG. 6. Large-area (001) plan view TEM micrographs of sample 3 allowing us to evaluate the MD density along the two ⟨110⟩ directions.

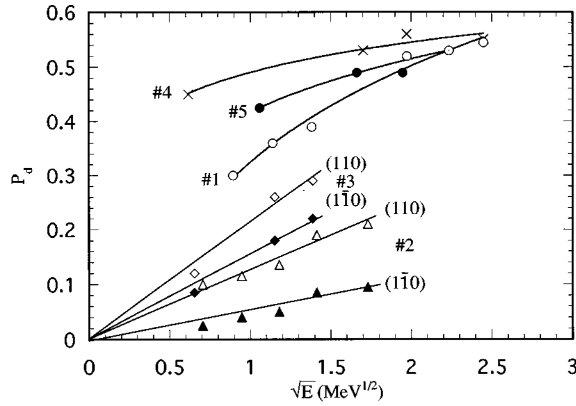

FIG. 7. The {110} planar dechanneling probability as a function of the square root of the He beam energy for the investigated samples. The specific channelling plane is indicated for samples where the (110) and (1$\bar{1}$0) directions gave rise to different dechanneling yields. The lines through the data points are drawn only to guide the eye. Sample 1, ○; sample 2, (110) and (1$\bar{1}$0), respectively, △ and ▲; sample 3, (110) and (1$\bar{1}$0), respectively, ◇ and ◆; sample 4, ×; sample 5, ●.

Theoretical dechanneling models predict that the dechanneling probability should depend linearly on the square root of the beam energy[6–9] until complete dechanneling ($P_d = 1$) is reached. Figure 7 reports the experimental results of our samples. It is evident that the linear behavior is followed only by samples with low dislocation densities. In fact, the dechanneling probability for samples 1, 4, and 5 saturates at a level of $P_d \sim \frac{1}{2}$. Some authors[11,19,20] have already discussed the so-called transparency effect: near the dislocation core, where the distortion of the lattice planes is high, the ion trajectory could cross the atomic plane and just become channeled in adjacent planar channels. However, such an effect cannot account, by itself, for such a large reduction of the dechanneling.

As a matter of fact, this low saturation value of the dechanneling probability is related to the nearly planar distribution of the dislocations. In fact, in the case of depth-distributed dislocations the dechanneling probability does saturate at $P_d = 1$. In Fig. 8 the TEM cross section of a $In_xGa_{1-x}As/GaAs$ step-graded composition buffer layer is presented. This buffer layer is made of five layers each 200 nm thick while the sixth (top) layer is 400 nm thick. The In concentration increases from $x = 0.085$ at a substrate interface to $x = 0.225$ at the surface in steps of variable amplitude. From Fig. 8 it appears that dislocations are present at each interface; and, in addition, some of them thread through the individual layers. The (110) planar channeling spectrum of this sample recorded with a 4-MeV He beam is shown in Fig. 9 together with the corresponding random spectrum. As the aligned yield reaches the random yield, it clearly appears that total dechanneling ($P_d = 1$) is achieved.

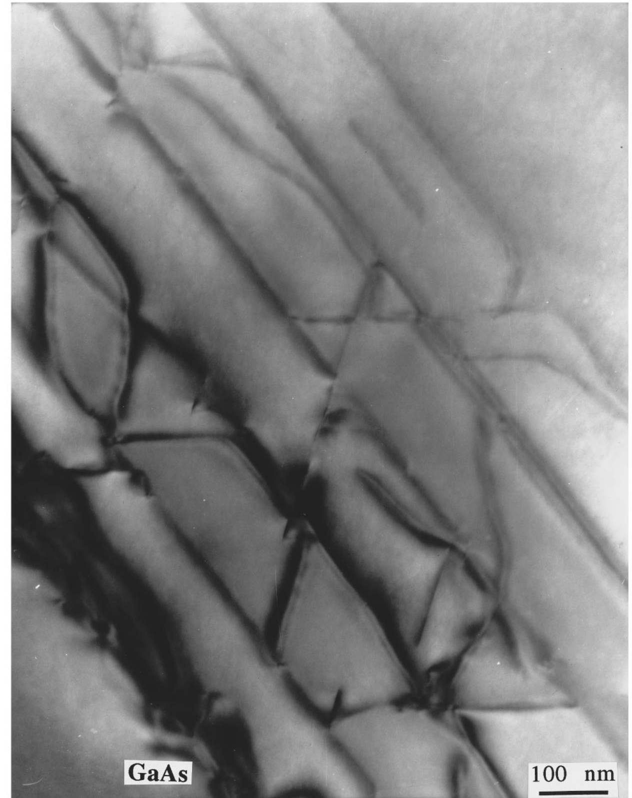

FIG. 8. [110] cross-section TEM image of a step-graded buffer layer of $In_xGa_{1-x}As/GaAs$ with x varying from 0.085 to 0.225 from the heterointerface to the top of the layer: the dislocations appear at each interface and also propagate across the layers.

TABLE II. Parameters used for the harmonic approximation to the planar Moliére potential. u_1 is the one-dimensional Debye thermal vibration amplitude, $x_{\lim}$ is the critical oscillation amplitude, d is the interplanar spacing, and K is the fitting harmonic potential parameter.

	u_1(nm)	$d/2-x_{\lim}$(nm)	$x_{\lim}$(nm)	$\sqrt{K/2}$ (10^6 MeV$^{1/2}$ cm^{-1})
GaAs	0.085	0.0092	0.0907	0.7188
GaP	0.0088	0.0094	0.0869	0.6904
InSb	0.0128	0.0128	0.1017	0.6122
Si	0.0075	0.0084	0.0876	0.5784

IV. DECHANNELING MODEL

A great deal of work has been devoted already to the development of phenomenological models of dechanneling. For a wide range of applications the "force balancing" model originally proposed by Quéré and co-worker[6,9] has been proved to be a satisfactory approach. On the basis of this approach the case of dechanneling by misfit dislocations in epitaxial heterostructures has been already analyzed.[21] In particular, it has been shown that the dechanneling cross section can be written as the product of a purely geometrical term and a physical term that contains the details of the confining potential and the incident ion energy. The geometrical term predicts the behavior of the dechanneling probability for different channeling configurations, i.e., the variation of the dechanneling rate as a function of both the angle between the dislocation line and the channeling plane and of the angle between the dislocation line and the channeling direction within the plane. This approach, where the plastic distortion field due to a dislocation is taken into account only through

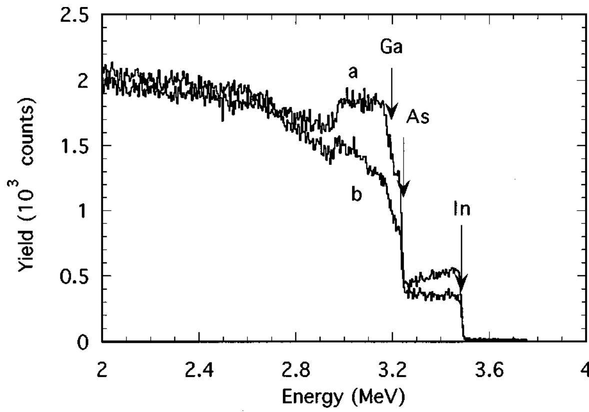

FIG. 9. 4-MeV He RBS spectra of the step-graded buffer layer of Fig. 8. Spectra *a* and *b* correspond to random and (110) incidence, respectively. Arrows indicate energies for surface scattering from different elements.

the peak value of the induced curvature,[6,9] cannot predict a saturation level below 100%.

Only models based on the dynamics of the ions in the channels can explain this effect, as already shown in the case of dechanneling by dislocation loops in axial channeling configuration.[22,23] Then, our previous model[21] has been modified toward a dynamic approach whose main characteristics are the following.

(i) Only planar channeling is considered, for two reasons. As is well known and as is shown in Fig. 4, planar channeling is more sensitive to dislocations than axial channeling. Moreover, planar channeling is sensitive to the dislocation line orientation as shown in the preceding section.

(ii) The dislocation distribution is supposed to be two dimensional. In other words, it is assumed that each channeled ion can perform at most one interaction event with the dislocations along the trajectory.

(iii) The actual confining potential is approximated by means of a harmonic potential. The deviation from the harmonic behavior will be discussed and taken into account.

The present model builds on the general approach introduced by Lindard and Bonderup *et al.*, who were the first to propose a description of dechanneling phenomena in terms of the amplitude of the oscillating ion trajectory.[24,25]

A. Normalized backscattering probability

It is well established that the motion of a channeled ion may be divided in two main components. The projection of the actual trajectory on the channeling plane will be called the longitudinal motion. The remaining component is the so-called transverse motion that is relevant for dechanneling. The transverse motion is the projection of the ion trajectory on the normal to the channeling plane and the solution of this one-dimensional motion is sufficient to determine the dechanneling probability. Even in a perfect crystal dechanneling occurs because of small-angle scattering events between the channeled ion and the atomic nuclei of the crystal lattice and between the ions and the electrons in the channels. Additional scattering events occur in the presence of lattice defects, like dislocations, and the total dechanneling probability is the result of the combined effects of these scattering mechanisms and of the defect contribution, including any possible correlation between them. Nevertheless here we consider the case of a quasiplanar distribution of defects whose influence on dechanneling is limited to a thin region where it dominates over the other contributions. For this reason the dechanneling probability (the interesting quantity from the experimental point of view) will be calculated by considering only the dislocation effect and by neglecting the scattering due to electrons and thermal vibrations. The dechanneling probability is defined as the change of the aligned normalized yield (as a result of the crossing of the dislocation grid) divided by the fraction of the originally channeled beam.

Let x be the coordinate describing the transverse motion and let the origin be at the center of the channel. The planar potential $U_{pv}(x)$ (index v indicates that atom vibrations about their lattice equilibrium positions are considered) is calculated by summing up the continuum Moliére potential calculated for the four nearest-neighbor atomic planes and by setting $U_{pv}(0)=0$. As usual the transverse energy is defined as the sum of the potential energy and of the transverse kinetic energy $m\dot{x}^2/2$. If no additional (external) force is present, the transverse energy of the ion probe is conserved, i.e., the particle oscillates between two neighboring atomic planes with constant amplitude. The lower the amplitude of the oscillation, the lower the probability of backscattering events between the incoming ion and a lattice nucleus. This effect is quantitatively described by introducing the so-called close-encounter collision probability Π, i.e., the probability of backscattering normalized to the random case. Due to their thermal vibration, the lattice nuclei are assumed to be statistically and isotropically distributed about their equilibrium position, the distribution being a Gaussian whose standard deviation σ is the one-dimensional thermal vibration amplitude u_1. If d is the interplanar spacing and X is the amplitude of the transverse motion we have

$$\Pi(X)=\frac{1}{d}\,\frac{\int_0^X 1/\sigma\sqrt{2\pi}\exp(-(d/2-x')^2/2\sigma^2)dx'/\sqrt{U_{pv}(X)-U_{pv}(x')}}{\int_0^X dx'/\sqrt{U_{pv}(X)-U_{pv}(x')}}. \tag{1}$$

From the close-encounter probability, the normalized channeling yield can be calculated by integrating over the amplitude distribution.

In our approach a channeled particle becomes dechanneled when its close-encounter probability reaches 100%. Through Eq. (1) this definition is equivalent to define a critical amplitude of the transverse motion $x_{\lim}$, or a critical transverse energy $E_{\perp}^{c}=U_{pv}(x_{\lim})$. However, it must be stressed that here the critical distance of approach depends on the actual planar potential as shown by the values reported in Table II for different materials. From this data it appears, in any case, that its value is quite reasonable as it turns out always to be $(d/2-x_{\lim})\approx\sigma$. Although Π can be greater than 1 for $x_{\lim}<x<d/2$, or, equivalently, for $E_{\perp}^{c}<E_{\perp}<U_{pv}(d/2)$, it is reasonable to assume that in this condition, which may eventually be determined by the abrupt energy variation due to the dislocations, any residual coherence of the transverse motion of the particles is easily wiped out. In fact, the energy $\Delta E=[U_{pv}(d/2)-E_{\perp}^{c}]$ is small enough to be promptly supplied by the highly probable scattering events between the ions and the lattice nuclei even if they are small-angle events. Therefore, the critical amplitude $x_{\lim}$ introduced here is just a cutoff parameter for the validity of the continuum potential approximation and it is not to be confused with the critical distance in the simple two-beam picture of channeling.

B. The harmonic approximation

As anticipated, the main approximation of this model concerns the form of the confining potential U. Following other authors the actual potential $U_{pv}(x)$ is approximated by means of a harmonic potential $U_h(x)=Kx^2/2$, which makes possible a crucial simplification of the form of the equation of motion for the channeled particles. The accuracy of this approximation is limited by the nonharmonicity of the actual potential U_{pv} mainly around the critical energy $E_{\perp}^{c}$. This problem has already been treated by other authors and, in particular, by Gartner, Hehl, and Schlotzhauer.[11] In order to provide the suitable approximation for our problem we proceed as follows: the dechanneling process is considered in terms of transverse energy variation. In other words, if the transverse energy of a particle changes from $E_{\perp}$ (before) to $E_{\perp}$ (after) as a consequence of the interaction with the dislocation, the dechanneling probability of the particle must increase by a quantity $\Delta\Pi=\Pi[E_{\perp}(\text{after})]-\Pi[E_{\perp}(\text{before})]$. By defining a virtual amplitude X_h for the harmonic oscillating motion such that $E_{\perp}=KX_h^2/2$, complete dechanneling ($\Pi=1$) is achieved for a critical virtual amplitude X_{hc}, given by

$$E_{\perp}^{c}=U_{pv}(x_{\lim})=U_h(X_{hc})=\frac{K}{2}X_{hc}^2. \tag{2}$$

It follows that both the harmonic parameter K and the critical virtual amplitude are related to the critical transverse energy so that another condition is needed in order to specify the approximation. This condition concerns the oscillation period due to the confining potential. In the harmonic case it is a constant given by

$$T_h=2\pi\sqrt{m/K}=\pi\sqrt{2m}\frac{X_{hc}}{\sqrt{E_{\perp}^{c}}}, \tag{3}$$

where m is the mass of the ion probe. Under the actual potential U_{pv} the period depends on the oscillation amplitude, i.e.,

$$T(X)=4\sqrt{m}\int_0^X\frac{dx'}{\sqrt{2[U_{pv}(X)-U_{pv}(x')]}}. \tag{4}$$

The oscillation period fixes the time scale for the interaction with the external force and consequently the average transverse momentum variation. Since the period depends on the oscillation amplitude, the equation of motion could be solved only by numerical methods. In order to deal with the problem in an analytical way, the natural approximation is to equate T_h to the average value of T between $X=0$ and $X=x_{\lim}$. Actually, since particles starting with amplitudes X close to $x_{\lim}$ can vary their dechanneling probability less than the well-channeled ($\Pi=0$) ones, we calculate the weighted mean of T as follows:

$$\langle T\rangle=\frac{\int_0^{x_{\lim}}[1-\Pi(X)]T(X)dX}{\int_0^{x_{\lim}}[1-\Pi(X)]dX}. \tag{5}$$

The condition $T_h=\langle T\rangle$ gives

$$x_{hc}=\frac{1}{2\pi}\sqrt{E_{\perp}^{c}/m}\langle T\rangle. \tag{6}$$

In summary, Eqs. (2) and (6) give the condition for the harmonic approximation of the confining potential. From now on we will drop the index h of the virtual coordinate x_h and we will call it the ''transverse position'' of the particle even if it is not the actual transverse coordinate.

C. Lattice distortion and perturbation to the harmonic oscillation

Following most of the literature on this topic, the dislocation distortion field is taken into account by considering a centripetal force acting on the traveling ions in the frame of reference of the channel. The force at a given point is $f=mv^2C$, where v is the ion longitudinal velocity and C is the effective curvature of the channeling plane at that point. It is called effective curvature since the component within the channeling plane of the displacement field generated by the dislocation does not affect the motion of the incoming ion, at least in the linear approximation of the elasticity theory. Then the equation of motion for a channeled ion is

$$\frac{d^2x}{dt^2}=-\frac{K}{m}x+v^2C. \tag{7}$$

The curvature C depends on the elastic distortion field generated by the dislocations, which in turn is strongly related to the geometric layout, i.e., to the orientation of the dislocations and their Burgers vectors with respect to the channel. In principle, it is possible to calculate C for any dislocation configuration by summing one by one the elastic distortion fields of all the dislocations. The effective curva-

ture C due to one dislocation having given orientation and Burgers vector and for a given longitudinal trajectory belonging to a given channeling plane is calculated in Appendix A.

The result may be expressed as follows:

$$C(z)=\frac{B}{\tau_0^2}\chi\left[\arctan\left(\xi\frac{zT_2}{r_0}\right)\right], \tag{8}$$

where z is the spatial coordinate of the longitudinal motion, B is the magnitude of the Burgers vector, r_0 is the impact parameter with the dislocation, T_2 is the component of the channeling direction perpendicular to the dislocation line, and $\xi=\pm1$. The function χ, which we call the distortion function, is dimensionless and does not depend on the physical quantities that are relevant for dechanneling, namely, the confining potential and the longitudinal beam energy [see Eq. (A8)].

If, as a first-order approximation the energy loss is neglected, it is possible to write $z=vt$, where v is the longitudinal velocity. Having defined $E=mv^2/2$, it is convenient to introduce the following reduced variables:

$$y=\frac{x}{X_c},$$

$$\omega=\frac{r_0}{\sqrt{E}}, \tag{9}$$

$$\tau=\frac{vt\sqrt{E_\perp^c}}{r_0X_c}.$$

Then Eqs. (7) and (8) give

$$\frac{d^2y}{d\tau^2}+\omega^2y=\hat{\chi}(\tau)\frac{BX_c}{E_\perp^c} \tag{10}$$

and

$$\hat{\chi}(\tau)=\chi\left[\arctan\left(\frac{\xi\tau}{\tau_c}\right)\right], \tag{11a}$$

$$\tau_c=\frac{\sqrt{E_\perp^c}}{T_2X_c}. \tag{11b}$$

It is useful to bear in mind that, according to the statement at the end of Sec. IV B, X_c is the critical virtual amplitude [Eq. (6)].

In Eq. (10) a channeled particle corresponds to the condition $-1<y<1$. The information concerning the material, the channeling configuration, and the dislocation are contained in the last term of the differential equation. The critical elongation X_c affects not only the amplitude of the external force but also the time scale of the interaction as it appears from Eq. (11). Incidentally, we can see that the argument of the function arctan in this equation is proportional to T_h, as expressed by Eq. (3), supporting the harmonic approximation to the potential introduced in Sec. IV B.

The integral of Eq. (10) is given by the sum of the general solution of the homogeneous equation and of a particular solution. Of course, the general solution is the equation of motion of a free harmonic oscillator

$$y_0(\tau)=Y\cos(\omega\tau+\Phi), \tag{12}$$

where Y and Φ are the oscillator normalized amplitude and phase, respectively. In order to find a particular solution of Eq. (10), the function $\hat{\chi}$ is expanded into Fourier series such as

$$\hat{\chi}(\tau)=\int_{-\infty}^{+\infty}\hat{\chi}(k)\exp(ik\tau)dk. \tag{13}$$

Under the action of the external force, for the particular normal mode $\exp(ik\tau)$, the harmonic oscillator tends to reach a steady state described by the function

$$y_k(\tau)=\frac{\exp(ik\tau)}{\omega^2-k^2}. \tag{14}$$

Since Eq. (10) is linear, the superposition principle guarantees that the particular solution is given by

$$y_p(\tau)=\frac{BX_c}{E_\perp^c}\int_{-\infty}^{+\infty}\hat{\chi}(k)\frac{\exp(ik\tau)}{\omega^2-k^2}dk, \tag{15}$$

so that the general integral of the equation of motion is

$$\begin{aligned}y(\tau)&=y_p(\tau)+y_0(\tau)\\&=y_p(\tau)+Y\cos(\omega\tau+\Phi).\end{aligned} \tag{16}$$

The problem is thus reduced to the calculation of the integral in Eq. (15). The function χ in Eq. (15) depends on the nature of the dislocation line and on the geometric layout of the experimental situation. The calculation of χ for two important configurations, which will be analyzed in detail in the next section, is reported in Appendix B. Although these configurations, described by the functions χ_e and χ_s, represent two limiting cases, any configuration of interest can be described by a linear combination of these two functions. For both χ_e and χ_s, the integral in Eq. (15) can be performed analytically by means of the theorem of residuals. The asymptotic behavior, for $\tau\to+\infty$, has a close form given by

$$\begin{aligned}y_p^e(\tau)=&\frac{B}{2X_c}[b_1(1+\eta\omega\tau_c)\cos(\omega\tau)\\&+\xi b_2(1-\eta+\eta\omega\tau_c)\sin(\omega\tau)]\exp(-\omega\tau_c),\end{aligned} \tag{17}$$

$$y_p^s(\tau)=\frac{B}{2T_2^2X_c}b_s\cos(\omega\tau)\exp(-\omega\tau_c),$$

for χ_e and χ_s, respectively, and with the meaning of symbols defined in Appendix A. In the special case of $T_2=1$ these results agree with that in Ref. 11. It is worth noting that the asymptotic effect of the perturbation is to introduce new terms having the same periodicity of the free harmonic oscillator [Eq. (12)]. A comparison between the numerical solution of Eq. (15) and the asymptotic analytical form given

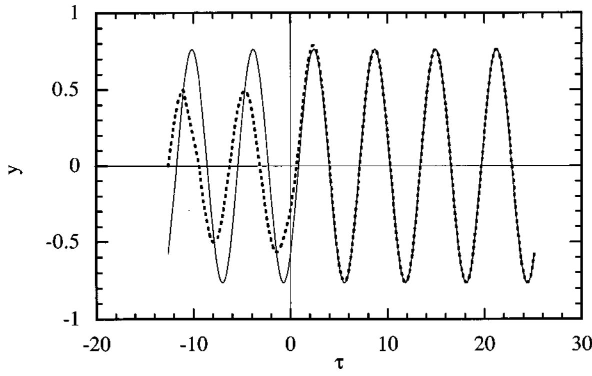

FIG. 10. Comparison of the asymptotic analytical solution (solid line) and of the numerical complete solution (dots) of Eq. (15) for a particular set of initial conditions.

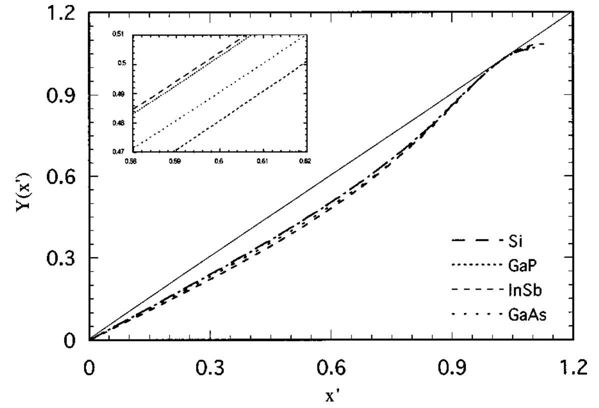

FIG. 11. Comparison of the distribution of the normalized harmonic amplitude for different materials as a function of the normalized impact coordinate. The inset shows the central part to better appreciate the small difference between the curves relative to different semiconductors as indicated in the figure. The full line represents the uniform distribution of impact parameters with respect to the Moliére potential.

by Eq. (17) shows that the two solutions are indistinguishable when the system completes at most one oscillation after the action of the perturbation. This point is illustrated in Fig. 10 for a particular set of initial conditions; however, the displayed behavior is of general validity.

According to Eqs. (17), the general form of the complete solution of Eq. (10) for any configuration, can be written as

$$y(\tau)=Y_f\cos(\omega\tau+\Phi_f), \tag{18}$$

where Y_f and Φ_f, which are functions of the initial conditions Y and Φ, are the amplitude and the phase of the oscillation after the perturbation. As we assume that statistical equilibrium is reached before the ions enter the distorted region, the initial phase is uniformly distributed. On the other hand, since the close-encounter probability is a function of the amplitude of the harmonic oscillator [see Eq. (1)], the relevant quantity for the calculation of the dechanneling probability is just the function $Y_f(Y,\Phi)$ and the statistical distribution of the initial amplitudes.

The distribution of the initial amplitudes is determined by the form of the actual confining potential when the incoming ions cross the free surface of the crystal.[26] In our harmonic approximation the initial amplitudes are calculated as follows: x is the actual impact coordinate which is uniformly distributed in the interval $[-x_{\rm lim},x_{\rm lim}]$. In order to preserve the actual transverse energy distribution, the normalized harmonic amplitudes Y are obtained by requiring that the harmonic oscillator energy is equal to the actual transverse energy of the incoming ion:

$$\begin{aligned} Y(x)&=\frac{X}{X_c}\\ &=\sqrt{U_{pv}(x)/E_\perp^c}\\ &=\sqrt{U_{pv}(x)/U_{pv}(x_{\rm lim})}. \end{aligned} \tag{19}$$

The function Y is reported in Fig. 11 as a function of the normalized coordinate $x'=x/x_{\rm lim}$. It is worth noting that it deviates substantially from the linear relationship resulting for a uniform distribution of impact parameters on the harmonic potential, showing the importance of the anharmonicity. In our approximation the harmonic parameter K depends on the material (lattice parameter and thermal vibration amplitude) as shown in Table II. Nevertheless the distribution of normalized harmonic amplitudes is nearly material independent as shown in Fig. 11. As a matter of fact the difference in the distribution for different materials amounts to a maximum of $\pm3\%$ and must be compared to the difference with respect to the harmonic distribution, which amounts to more than 20%.

The actual amplitude distribution just before the dislocations should be calculated by taking into account the modifications in the surface amplitude distribution that are induced by the dechanneling processes occurring in a defect-free crystal. However, we neglect these processes in our model since we are interested in epitaxial structures where the epilayer-substrate interface is located, at most, several hundred nanometers below the surface.

In conclusion, if G is the inverse function of Y, the dechanneling probability for a given value of ω, $f(\omega)$, can be calculated as follows:

$$f(\omega)=\frac{\int_0^1 dY\int_0^{2\pi}d\Phi\{\Pi[X_cY_f(Y,\Phi)]-\Pi(X_cY)\}G'(Y)}{\int_0^1 dY\int_0^{2\pi}d\Phi[1-\Pi(X_cY)]G'(Y)}. \tag{20}$$

Since $\omega=r_0/\sqrt{E}$, i.e., for a given value of the beam energy the ``pulse'' is proportional to the impact parameter r_0, the integral dechanneling probability P_d for a uniform distribution of impact parameters must be computed by integrating $f(\omega)$ over the interval $[0,\omega_{\rm max}=r_0^{\rm max}/\sqrt{E}]$ where $r_0^{\rm max}$ is a suitable cutoff parameter beyond which the dechanneling contribution becomes negligible. This cutoff parameter shall depend on the specific dislocation configuration as presented in the next subsection. In order to obtain P_d by the integration of $f(\omega)$, the calculation procedure for $f(\omega)$ is repeated for a set of different (significant) values of ω and then $f(\omega)$ is determined by interpolation over the specified interval.

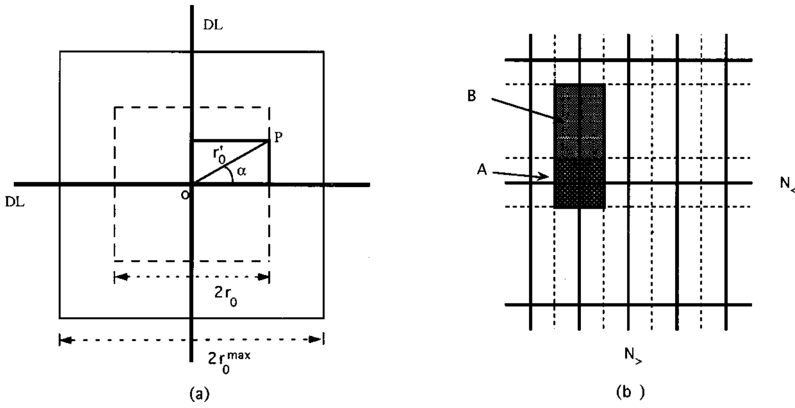

FIG. 12. Geometry for the calculation of the dechanneling probability of two orthogonal arrays of dislocations lines (DL's): (a) two crossing dislocations; (b) two arrays of DL's with different densities ($N_>$ and $N_<$). The heavy continuous lines represent the dislocation lines. The shaded rectangle represents the integration area, which is divided into regions A and B for the 2D and 1D integration types, respectively.

D. Solutions for specific dislocation configurations

The effect of typical configurations that are more frequently found in low misfit heterostructures may be obtained by considering separately two elemental cases: (i) the interaction between the ion beam and the lattice distortion caused by an array of parallel dislocations; (ii) the effect of two crossing dislocations and the generalization to two crossing arrays of parallel dislocations.

In the case of a planar distribution of parallel dislocations, we assume that $2r_0^{max}=N^{-1}$, where N is the (average) dislocation density per unit length. The dechanneling probability, P_d^{1D}, for this array (one-dimensional array) is then given by

$$P_d^{1D}(\chi,\omega_{max})=P_d^{1D}(\chi,r_0^{max}/\sqrt{E})=\frac{1}{r_0^{max}}\int_0^{r_0^{max}}f(\omega)dr_0=\frac{1}{\omega_{max}}\int_0^{\omega_{max}}f(\omega)d\omega, \tag{21}$$

where χ is reported as a label to indicate the geometrical configuration.

Since $\omega_{max}=r_0^{max}/\sqrt{E}=1/(2N\sqrt{E})$, Eq. (21) gives P_d^{1D} as a function of $N\sqrt{E}$. That shows that different samples of the same material, having different dislocation densities, will exhibit the same dechanneling probability at an energy value that is scaled as the inverse of the square of the dislocation densities. This result will be later applied to study one couple of channeling configurations particularly suitable for the study of MD's because of the particular features shown by the resulting dechanneling probability functions.

Before doing this, let us consider the case (ii) of two crossing dislocations. Despite the fact that there is no limit to generalization, the calculation will be restricted to the particular case of perpendicular dislocations, corresponding to the experimental situation in [001]-grown heterostructures. This is done to avoid cumbersome formulas and notations that would be scarcely significant in this context. Moreover, for the sake of simplicity, we suppose that the direction of the incident beam, i.e., the unit vector $\mathbf{T}$, is perpendicular to the plane p containing the dislocations ($T_2=1$). Actually, as it is discussed in Appendix B, most of the experimental configurations that are used for dechanneling analysis are quite close to this situation.

Figure 12(a) shows the plane p of the dislocations and the polar frame of reference whose origin is at the dislocation node O. A square, centered at O, whose side length is $2r_0^{max}$ is considered. A point P inside the square defines two impact parameters of the beam with the two crossing dislocations, i.e., $r_0'\cos\alpha$ and $r_0'\sin\alpha$ [see Fig. 12(a)]. The distortion field is the sum of the fields of the two dislocations and, owing to the linear approximation in the calculation of the total curvature (Appendix A), the equation of motion [Eq. (10)] becomes

$$\frac{d^2y}{d\tau^2}=-\omega_\alpha^2y+\frac{BX_c}{E_\perp^c}\left[\frac{\chi_a(\phi)}{\cos^2\alpha}+\frac{\chi_b(\phi')}{\sin^2\alpha}\right],$$

$$\omega_\alpha=\frac{r_0'}{\sqrt{E}},$$

$$\phi=\arctan\left(\frac{\tau}{\tau_c\cos\alpha}\right),$$

$$\phi'=\arctan\left(\frac{\tau}{\tau_c\sin\alpha}\right), \tag{22}$$

$$r_0'=\frac{r_0}{\max(|\cos\alpha|,|\sin\alpha|)},$$

where α is the angle defined in Fig. 12(a). Equations (22) are solved in the same way as Eq. (10) with the difference that in this case the dechanneling probability for the given impact point P obtained by Eq. (20), $f_2(r_0,\alpha)$, is a function of the two parameters r_0 and $\alpha(0<\alpha<2\pi$ and $0<r_0<r_{max})$. Analogously to what has been done for case (i), a uniform distribution of r_0 within the interval $[0,r_0^{max}]$ is assumed and $\omega_{max}=r_0^{max}/\sqrt{E}$ is defined. Then the total dechanneling probability P_d^{2D} can be calculated by averaging f_2 over the square of side r_0^{max}:

$$P_d^{2D}(\chi_a,\chi_b,\omega_{max})=\frac{1}{2\pi(2r_0^{max})^2}\int_0^{r_0^{max}}8r_0dr_0\int_0^{2\pi}d\alpha\, f_2(r_0,\alpha)=\frac{1}{\pi\omega_{max}^2}\int_0^{\omega_{max}}\omega_\alpha d\omega_\alpha\int_0^{2\pi}d\alpha\, f_2(r_0,\alpha). \tag{23}$$

If the dislocations are arranged in a network of two perpendicular arrays, both characterized by the same (average) dislocation density per unit length N it can be set $2r_0^{\max}=N^{-1}$ and also $P_d^{2\mathrm{D}}$ is given as a function of $N\sqrt{E}$.

In order to obtain the total dechanneling probability in the case of different dislocation densities in the two arrays, the plane containing the dislocations is divided into rectangular cells as shown in Fig. 12(b). The sides of the rectangle have length equal to $N_>^{-1}$and $N_<^{-1}$ where $N_>$ ($N_<$) are the highest (lowest) of the two dislocation densities. Each unit cell is composed of a square region (A) and a rectangular region (B). It is assumed that in region A the interaction with the two dislocations, which cross at the center of the region, dominates over the effects due to all the other dislocations, so that the dechanneling probability is given by Eq. (23). On the other hand, in region B only the effects due to the dislocations in the highest-density direction are supposed to be effective. The total dechanneling probability is then the weighted average between the 1D probability of region B and the 2D probability of region A. This is summarized by

$$P_d^i\left(N_>\sqrt{E},\frac{N_<}{N_>}\right)=\frac{N_<}{N_>}P_d^{2\mathrm{D}}(\chi_a,\chi_b,\omega_{\max})+\left(1-\frac{N_<}{N_>}\right)P_d^{1\mathrm{D}}(\chi_i,\omega_{\max}),\quad(24)$$

where P_d^i $(i=a,b)$ is the total dechanneling probability when the densest dislocations are in configuration χ_a or χ_b, and

$$\omega_{\max}=2N_>\sqrt{E}.\quad(25)$$

Experimentally P_d^a and P_d^b can be measured by changing the channeling plane in such a way that the high-density dislocation array is either in configuration χ_a or χ_b. Of course the low-density dislocation array in then in configuration χ_b or χ_a, respectively. Equation (24) also shows the way to measure both $N_>$ and $N_<$. In fact, for a given ratio of the dislocation densities $N_</N_>$, the difference between P_d^a and P_d^b is greater the higher the difference between $P_d^{1\mathrm{D}}(\chi_a)$and $P_d^{1\mathrm{D}}(\chi_b)$. For this reason the best combination of channeling configurations is the one providing the highest difference between the average magnitude of the corresponding distortion functions.

Appendix B reports the calculation of the distortion function for two configurations. The first one is the case of a dislocation perpendicular to the channeling plane. We name it screw configuration (s) since the corresponding distortion function χ_s depends only on the screw component of the Burgers vector. In the second case, the edge configuration (e), the dislocation direction belongs to the channeling plane and the distortion function χ_e depends only on the edge component of the Burgers vector. These are possible configurations in (001)-grown heterostructures where misfit dislocations are $\langle 110\rangle$ oriented and the couple of $\{110\}$ planes perpendicular to the interface are either perpendicular or parallel to the dislocation lines. These planes are also convenient from the channeling point of view because the atomic sheets are equally spaced and mixed (i.e., they contain both anions and cations). Moreover, for these planes both the minimum yield and the dechanneling rate for a perfect crystal are low. In addition, as calculated in Appendix B and shown in Fig. 17, the ratio of the maximum amplitude of the two distortion functions $\chi_e^{\max}/\chi_s^{\max}$ is greater than 4.5 for all the cubic semiconductors. As a consequence, the ratio R between the dechanneling probability for configurations e and s is particularly high and small asymmetries in the dislocation distribution can be detected by using these channeling planes.

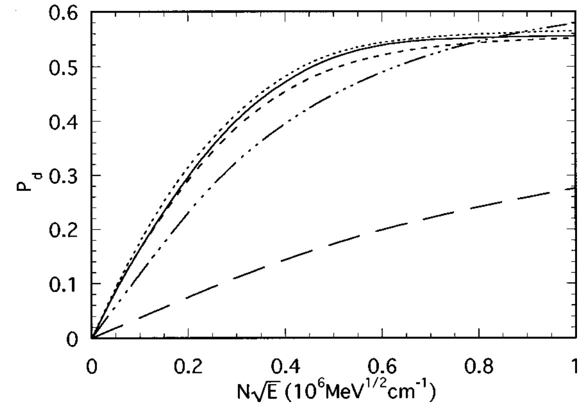

FIG. 13. Computed (110) planar dechanneling probabilities for different configurations in GaAs as a function of $\omega^{-1}=N\sqrt{E}$: $P_d^{1\mathrm{D}}(\chi_s)$ (long-dashed line); $P_d^{1\mathrm{D}}(\chi_e)$ (dash-dotted line). $P_d^{2\mathrm{D}}(\chi_s,\chi_e)$ has been computed for different thermal vibration amplitudes: $u_1=0.0085$ nm (solid line); $u_1=0.0075$ nm (short-dashed line); $u_1=0.0095$ nm (dotted line).

The calculated $P_d^{1\mathrm{D}}(\chi_e)$, $P_d^{1\mathrm{D}}(\chi_s)$, and $P_d^{2\mathrm{D}}(\chi_s,\chi_e)$, for GaAs $\{110\}$ channeling planes, are reported in Fig. 13 as a function of $\omega^{-1}=N\sqrt{E}$. It can be seen that the ratio R varies about from 3 to 2 when $N\sqrt{E}$ increases over the displayed range. Within the range $0<N\sqrt{E}<0.3\times10^6$ MeV$^{1/2}$ cm^{-1} the dechanneling probability behaves almost linearly while for higher values it tends to saturate. The saturation effect is stronger for $P_d^{2\mathrm{D}}$,whose rate of change is quite negligible for $N\sqrt{E}>0.7\times10^6$ MeV$^{1/2}$ cm^{-1}. These features limit the range of dislocation densities that can be detected by dechanneling, the upper limit being fixed by the lowest beam energy compatible with the thickness h of the analyzed layer. For instance, $h\sim100$ nm requires $E_{\min}>0.5$ MeV and then $N_{\max}\sim1\times10^6$ cm^{-1}. On the other hand, since the uncertainty in the experimental determination of P_d is of the order of 0.03, for $E\sim6$ MeV we have $N_{\min}\sim10^4$ cm^{-1}, which is also the order of magnitude of the minimum detectable difference between the dislocation densities in the two $\langle 110\rangle$ directions.

In order to determine to what extent P_d varies by changing the atomic vibration amplitude, the 2D probability has been computed for different values of u_1. In fact experimental results[27] on GaAs thermal vibrations are discordant and range from u_1=0.025 Å to u_1=0.117 Å. The solid-line curve of Fig. 13 has been obtained by assuming for Ga and As atoms an average thermal oscillation amplitude $u_1=0.085$ Å as calculated by using the Debye model for Ge. This value is quite reasonable as it turns out to be also the average value of many computed and measured values of

u_1 as reported in Table I of Ref. 27. The values of $P_d^{2D}(\chi_s,\chi_e)$ computed for $u_1=0.075$ Å and for $u_1=0.095$ Å are also reported in Fig. 13. It appears that a variation of u_1 of about 25% gives rise to a P_d variation lower than 7%, so that the results of the dechanneling model are not too sensitive to the actual thermal vibration amplitude.

Finally, a few words about the depth range where dechanneling occurs. The transverse motion in the harmonic approximation is characterized by a wavelength given by

$$\begin{aligned}\lambda &= vT\\ &= 2\pi\sqrt{E/(K/2)}\\ &= 2\pi\frac{X_c}{\sqrt{E_\perp^c}}\sqrt{E}.\end{aligned}\tag{26}$$

On the other hand, the interaction with the dislocations is appreciable at a distance $|z|_{\max}$ given by

$$|z|_{\max}=\frac{|\tan\phi|_{\max}}{T_2}r_0.\tag{27}$$

From the data reported in Fig. 17 it appears that for GaAs {110}, it is $|\tan(\phi)|_{\max}\sim 2$. Then, by using the value of the harmonic constant reported in Table II, $|z|_{\max}/(\lambda/2)\approx 0.45r_0/\sqrt{E}=0.45\omega$, with ω in units of 10^6 cm $\text{MeV}^{-1/2}$. This means that for $\omega<2.2$, i.e., for most of the dechanneling events, dechanneling occurs essentially within half of the trajectory wavelength, in perfect agreement with the results of the numerical solution of the equation of motion (see Sec. IV C and Fig. 10). From Eq. (26) it turns out that $\lambda/2\approx 44\sqrt{E}$ nm with E in MeV. This quantity establishes a lower limit for the dislocation depth location by dechanneling. This limit can be higher than the intrinsic RBS resolution and is a conflicting parameter with respect to the sensitivity, which increases with increasing energy.

V. DISCUSSION

The dislocation densities for each of the investigated samples have been determined by comparing the experimental (110) planar dechanneling probabilities to the theoretical curves as discussed above. The results for samples with no asymmetry in the dislocation distribution are presented in Fig. 14 while Fig. 15 shows the (110) and $(1\bar{1}0)$ dechanneling probabilities for sample 2 exhibiting the highest asymmetry in the dislocation distribution. The only fitting parameter in this comparison is the dislocation density. The resulting values are presented in Table I, where the TEM data and the predictions given by the RBS-channeling tetragonal distortion measurements[12,28] are reported for comparison. The estimation of the dislocation density obtained from the tetragonal distortion is calculated by assuming that the in-plane strain is related to the tetragonal distortion as predicted by the isotropic elastic continuum model[29] and that only 60°-type MD are present.

From the comparison of the data in Table I it appears that the three techniques supply comparable results within their respective error bars (apart from sample 5, where the discrepancies are a bit larger than the combined errors). However, the experimental uncertainties for the three techniques are widely different and variable with the dislocation density. As for the TEM errors, in the present investigation we are concerned with low dislocation densities and the error bar can be reduced only by increasing the number of observed dislocations. This would require us to increase the examined sample area, and it must be stressed that in order to reduce the error bar by a factor 2 the examined area should be increased by a factor 16. The error bar in the data coming from the strain release measure is essentially dislocation density independent as it comes from the error in the tetragonal distortion measure (channeling) and from the error in the alloy composition (RBS). In our experimental setup they contribute a total of $\sim(3-5)\times 10^4$ cm^{-1}. Finally, the estimation of the error in the dechanneling measure comes from the half-dispersion of the data obtained for different beam energies. As a consequence of the saturation effect, the error may vary by more than one order of magnitude following the value of the dislocation density (see, for instance, samples 2 and 4). For this reason the comparison of the results is divided into low- and high-density regimes.

In the case of low-MD-density samples (2 and 3) (where also an asymmetry in the dislocation distribution is ob-

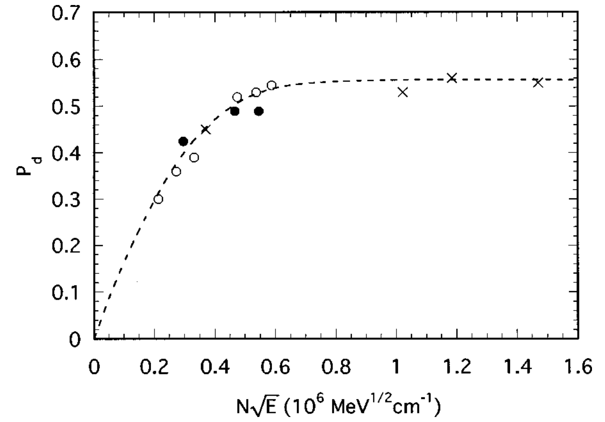

FIG. 14. Comparison between the experimental determination of the dechanneling probability for samples 1 (○), 4 (×), and 5 (●), showing no asymmetry in the dislocation distribution, and the model prediction for a square network of dislocations (dashed line).

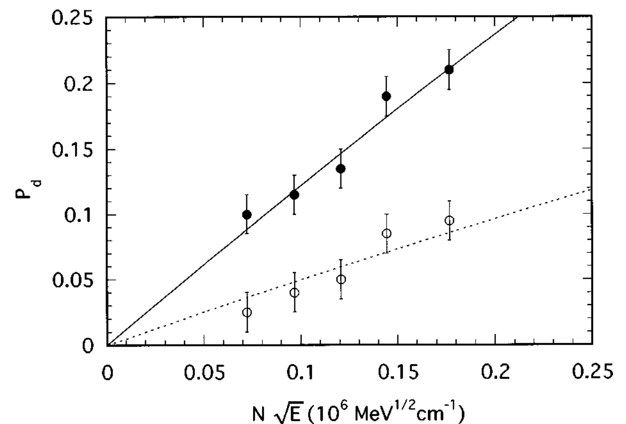

FIG. 15. The dechanneling probability of sample 2, showing asymmetry in the dislocation distribution, for (110) (●) and $(1\bar{1}0)$ (○) planar channeling and different beam energies. The lines through the data points are the result of fitting the model prediction.

served) the agreement between dechanneling and TEM data is surprisingly excellent in view of the fact that no adjustable parameters in the dechanneling model are present. Thus it appears that dechanneling is an accurate technique for the measure of relatively low dislocation densities. Moreover, it is very precise as its error bar is two times and one order of magnitude lower than those of the TEM and strain technique, respectively. Finally, dechanneling is also quite sensitive to the dislocation distribution (see Figs. 13 and 15) even though it is not an imaging technique.

In the high-density regime ($N>10^5$ cm^{-1}) the main result is the very good agreement between the predicted dechanneling saturation level $[P_d^{2D}(\chi_s,\chi_e)]$ and the experimental data as shown in Fig. 14. At the same time, dechanneling saturation causes large uncertainties in the measure of the MD density. Nevertheless, by comparing dechanneling and strain results, a systematic difference appears. This requires a detailed discussion.

One of the assumptions of the model is that dislocations are equally spaced in each array. Actually, this is not true, and the onset of a nonlinear dechanneling regime affects the accuracy of the dislocation density estimation. In fact, when two or more dislocations are closer than the saturation distance $d_s \sim 20\sqrt{E(\mathrm{MeV})}$ nm corresponding to the $N\sqrt{E}$ saturation value of about 0.5×10^6 MeV$^{1/2}$ cm^{-1} (see Fig. 13), they cannot be discriminated. This fact leads us to underestimate the average density. This effect is expected to be increasingly important with increasing dislocation density and it is a possible explanation for the discrepancies between the strain predictions and the dechanneling results. However, it should play a role also in the case of low dislocation densities, because of the occurrence of dislocation bands [see Fig. 1(a)], if the MD separation is of the order of (or lower than) d_s.

In any case, to complete the discussion on the relation between relaxed strain and MD density we must take into account the following points.

(i) TEM images show that dislocation dipoles are present in our samples (Fig. 2). They are generated through the interaction between crossing dislocations having proper Burgers vectors.[17] A dipole can be detected by dechanneling as one or two dislocation lines depending on the separation between the two dislocation branches. Since dipoles are ineffective in releasing strain, their presence would increase the number of MD's detected by dechanneling with respect to the value predicted by the relaxed strain data. However, acceptable statistics on the dipole densities could not be obtained by the TEM maps in agreement with energy minimization arguments, suggesting that the percentage of dislocation dipoles should not be significant.

(ii) Despite the fact that the overwhelming majority of MD's are of 60° type, the presence of pure edge dislocations, arising from the interaction between two 60° lines, is more probable the higher the overall MD density.[14] Each edge dislocation gives a double contribution to the strain relaxation with respect to a 60° one but, from the dechanneling point of view, the two types of dislocation are quite indistinguishable as the distortion function for the edge dislocation is comparable to χ_e. For this reason, the presence of many pure edge dislocations would give rise to discrepancies in the opposite direction with respect to item (i) and in the same direction shown by the experimental results. On the other hand, since our samples are low misfit ones and since TEM gives no evidence of a significant edge dislocation presence, this is not the probable explanation of the observed discrepancy.

(iii) The third point concerns the reliability of the relaxed strain data as obtained by RBS channeling. It has been demonstrated that RBS channeling and x-ray diffraction provide measurements of the tetragonal distortion of an epitaxial layer in perfect agreement.[30,31] In the case of RBS channeling, in order to obtain the in-plane strain $\varepsilon_{\parallel}$ the relation between $\varepsilon_{\parallel}$ and the perpendicular strain $\varepsilon_{\perp}$ arising from the isotropic elastic continuum model is assumed.[29] However, there are experimental data that contradict this assumption.[28,31] One possible explanation is related to the conservation of the bond lengths and to the consequent deformation of the angles between anion and cation bonds leading to significant deviations from the ideal zinc-blende lattice, particularly under epitaxial conditions. These ''internal'' degrees of freedom can give rise to a lower elastic energy density per unit volume and consequently to a lower tetragonal distortion[32] than is predicted in the frame of the virtual crystal approximation. As a matter of fact, the data of Fig. 8 of Ref. 28 show that, at high MD density, the strain relaxation determined by channeling is an overestimate with respect to that obtained by double crystal x-ray diffraction. The difference amounts to about $(2-6)\times 10^{-4}$ cm^{-1}, corresponding to an increase of the estimated MD density of about $(2-6)\times 10^4$ cm^{-1}, which compares very well with the difference of $(3-7)\times 10^4$ cm^{-1} between the strain and the dechanneling measure observed for samples 1, 4, and 5.

As far as the dechanneling model is concerned, we emphasize that its usefulness is strictly related to the well-defined geometry of the MD in semiconductor epitaxial heterostructures. In this respect, however, the present GaAs results can be easily extended to other materials. In fact, as shown in Fig. 11, the dependence of the results on the material parameters is very weak for all semiconductors (zinc-blende or diamond structures). In addition, the distortion functions calculated in this paper for GaAs are not much different from those of other materials, as the Burgers vectors and the Poisson ratio do not vary appreciably for different semiconductors. Moreover, the influence of the lattice vibrations, often not very well known, is weak as well.

VI. CONCLUSIONS

Quantitative and qualitative characterization of misfit dislocations at the interface between an epitaxial layer and the substrate has been carried out on a series of (001) grown $In_xGa_{1-x}As/GaAs$ low misfit samples by means of dechanneling and TEM. Planar channeling along the two {110} planes perpendicular to the interface has been performed at different ion-beam energies. The dechanneling probability due to the dislocations increases linearly with the square root of the energy until a saturation level of about $\frac{1}{2}$ is reached due to the quasiplanar distribution of the dislocations. Moreover, samples where TEM images show an asymmetric dislocation distribution exhibit a different dechanneling probability for the two mutually perpendicular channeling planes.

The latter effect is due to a sort of geometry-induced selection rule.

These experimental features are well accounted for by the planar dechanneling model presented in this paper. The proposed model is based on the harmonic approximation of the actual confining planar potential, the average contribution of the anharmonic terms to the dynamics of the particle being taken into account. The dechanneling probability is obtained by solving the equation of motion of the ions and by taking into account the statistical distribution of their transverse amplitudes. No adjustable parameter is present and the form of the equation of motion is such that all the essential information about the relative orientation of the dislocation and the channeling direction is contained in a single term called the distortion function. The model can be applied to all the possible orientations of the channeling plane with respect to the dislocation line. In this paper the calculation has been carried out for the case of misfit dislocations in (001)-grown heterostructures. The calculated dechanneling probabilities turn out to agree very well with the experimental results both at low and at high beam energy, where the saturation level is correctly predicted.

Supported by this model, the dechanneling technique becomes well adapted to determine the MD density and orientation. It is quantitative, non destructive, and its accuracy is of the same order of magnitude of the one obtained by large-area TEM micrographs. These features can give an important contribution toward the understanding of the mechanisms of strain relaxation. As a matter of fact, a single RBS-channeling experimental setup provides independent information on the alloy composition (misfit), the tetragonal distortion of the epitaxial film, and the misfit dislocation densities and orientations. That appears to be a powerful tool to investigate the role of plastic relaxation in misfit accommodation, which is crucial for throwing light on the still open general problem of the mechanism of elastic energy reduction in epitaxial heterostructures.

ACKNOWLEDGMENTS

The authors wish to thank F. Genova for growing the samples, C. Ferrari and P. Franzosi for the x-ray topography, and A. Carnera for many useful discussions. This work has been partly supported by the Finalized Project of CNR ''Special Materials for Advanced Technologies.''

APPENDIX A

Let $\mathbf{T}$ and $\mathbf{s}$ be unit vectors indicating the longitudinal direction of the ion trajectory and the opposite of the dislocation line orientation, respectively. On the plane $\mathbf{s}$, normal to $\mathbf{s}$, i.e., normal to the dislocation line), we take $\mathbf{e}_2$ to be the normalized projection of $\mathbf{T}$ on s and $\mathbf{e}_1$ such that $\mathbf{e}_1 = \mathbf{e}_2 \times \mathbf{s}$ (see Fig. 16) so that $\mathbf{e}_1$ is perpendicular to both the channeling direction and the dislocation line. If the distortion field due to the dislocation line were zero, the longitudinal motion of the channeled ion would be a straight line. By defining the origin O as the point on the dislocation line that is at the minimum distance from the longitudinal trajectory, its parametric equation is

$$\mathbf{r}(z) = \xi r_0 \mathbf{e}_1 + z\mathbf{T}, \tag{A1}$$

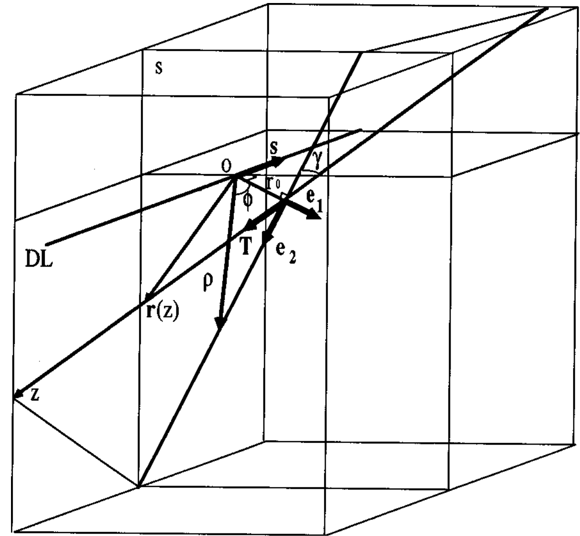

FIG. 16. Geometrical description for the most general configuration of a rectilinear dislocation line (DL) and of the ion trajectory ($\mathbf{T}$). The relationship between the rectangular frame of reference defined by the unit vectors $\mathbf{e}_1$, $\mathbf{e}_2$, and $\mathbf{s}$ and the cylindrical frame of reference (ρ,ϕ,s) is shown.

where r_0 is the impact parameter between the incident ion and the dislocation line, $\mathbf{r}(z)$ is the position vector, and z is the coordinate along $\mathbf{T}$ such that $r(0) = r_0 \xi = \pm 1$ gives the relative orientation of $\mathbf{r}(0)$ and $\mathbf{e}_1$.

The effect of the dislocation distortion field may be evaluated as follows. Within the linear elasticity theory, a point at a position $\mathbf{r}$ in an undistorted crystal is forced by the elastic distortion field to a position $\mathbf{r}' = \mathbf{r} + \mathbf{u}(\mathbf{r})$, where $\mathbf{u}$ is the elastic displacement vector. The result is a local bending of the atomic planes. As a consequence, the longitudinal direction $\mathbf{T}$ is locally tilted by an amount $\delta\mathbf{T} = d\mathbf{r}'/dz - \mathbf{T} = \bar{\bar{u}}\mathbf{T}$, where $\bar{\bar{u}}$ is the elastic distortion tensor whose components are given by $u_{ij} = \partial u_i / \partial x_j$. If $\mathbf{n}$ is the unit vector normal to the channeling plane the angular displacement in the transverse direction is given by $\mathbf{n}\cdot\delta\mathbf{T} = \mathbf{n}\cdot\bar{\bar{u}}\mathbf{T}$ and the effective curvature results:

$$C = \mathbf{n}\cdot\frac{d\,\delta\mathbf{T}}{dz} = \mathbf{n}\cdot\frac{d\bar{\bar{u}}}{dz}\mathbf{T}. \tag{A2}$$

The curvature $C(z)$ along the path $\mathbf{r}(z)$, that is, the behavior of the tensor $\bar{\bar{u}}$ along the straight line, must be determined. To this purpose the cylindrical coordinate system $(\rho,\phi,\mathbf{s})$ is considered whose symmetry axis is the dislocation line and the corresponding rectangular frame $(\mathbf{e}_1,\mathbf{e}_2,\mathbf{s})$. The distortion field $\bar{\bar{u}}$ does not vary along the direction of $\mathbf{s}$, i.e., it depends only on ρ and ϕ. Actually, it can be written as

$$\bar{\bar{u}} = \frac{B}{2\pi\rho}\bar{\bar{v}}(\mathbf{b},\phi), \tag{A3}$$

where $\mathbf{B} = (B_1, B_2, B_s)$ is the Burgers vector of the dislocation and $\mathbf{b} = \mathbf{B}/B$ is the unit vector parallel to $\mathbf{B}$. The components of the tensor $\bar{\bar{v}}$ are given by

$$v_{ss}=v_{1s}=v_{2s}=0,$$

$$v_{s1}=-b_s\sin\phi,$$

$$v_{11}=b_2\cos\phi(\eta\cos 2\phi-2\eta+1)-b_1\sin\phi(\eta\cos 2\phi+1),$$

$$v_{21}=(b_2\sin\phi+b_1\cos\phi)(1-\eta\cos 2\phi), \tag{A4}$$

$$v_{s2}=b_s\cos\phi,$$

$$v_{21}=(b_2\sin\phi+b_1\cos\phi)(1+\eta\cos 2\phi),$$

$$v_{22}=b_2\cos\phi(1-\eta\cos 2\phi)-b_1\sin\phi(1-\eta\cos 2\phi-2\eta),$$

where

$$\eta=\frac{1}{2}\left(\frac{1}{1-\nu}\right), \tag{A5}$$

and ν is the Poisson ratio of the material.

Since the distortion field is uniform in direction $\mathbf{s}$, the s component of $\mathbf{r}(z)$ is not relevant for the calculation of $C(z)$. The projection of the undistorted longitudinal path on the plane s is described by the equation

$$\rho(z)=\xi\mathbf{r}_0\mathbf{e}_1+zT_2\mathbf{e}_2, \tag{A6}$$

where $T_2=\mathbf{T}\cdot\mathbf{e}_2=\cos\gamma$ and $\rho(\phi)=|\rho(z)|=\xi\mathbf{r}_0/\cos\phi$.

(Note that $\xi>0$ if $\phi\in(-\pi/2,\pi/2)$ and $\xi<0$ if $\phi\in(-\pi/2,3\pi/2)$. The angle γ is the angle between the trajectory direction and its projection on the plane s perpendicular to the dislocation line (see Fig. 16). Equation (A3) becomes

$$\bar{\bar{u}}(z)=\frac{\xi B}{2\pi r_0}\bar{\bar{v}}(\mathbf{b},\phi)\cos\phi,$$
$$z=\xi\frac{r_0\tan\phi}{T_2}. \tag{A7}$$

Finally, by substituting Eq. (A7) into Eq. (A2), the effective curvature turns out to be

$$C(\phi)=\frac{d\phi}{dz}\mathbf{n}\cdot\frac{d\bar{\bar{u}}}{d\phi}\mathbf{T}$$
$$=\xi^2\frac{B}{r_0^2}\left[\frac{T_2\cos^2(\phi)}{2\pi}\mathbf{n}\cdot\frac{d}{d\phi}[\bar{\bar{v}}(\phi)\cos(\phi)]\mathbf{T}\right]$$
$$=\frac{B}{r_0^2}\chi(\phi). \tag{A8}$$

It is worth noting that the curvature is proportional to the ''distortion function'' $\chi(\phi)$, which depends only on the geometry of the problem, i.e., on the relative orientation of the dislocation line, Burgers vector, and channeling direction.

APPENDIX B

Here the distortion function χ is calculated for two configurations (specified by dislocation orientations, Burgers vector, channeling plane, and direction of the longitudinal trajectory) that correspond to a typical experimental layout for zinc-blende heterostructures. In (001)-grown heterostructures misfit dislocations lay in the $[110]$ and/or the $[1\bar{1}0]$ direction in the (001) interface plane and the $\{110\}$ channeling planes perpendicular to the interface are thus parallel (configuration e) or perpendicular (configuration s) to the dislocation lines. They are the most suitable channeling planes, as it will be shown in the following that they exhibit a high ratio $R=P_e^{1\mathrm{D}}/P_s^{1\mathrm{D}}$ between the dechanneling probabilities in the edge and the screw configurations. The distortion functions can be calculated from Eq. (A7):

$$\chi_e=\frac{\cos^2\gamma}{2\pi}\cos^2\phi\{b_2(\eta\cos 4\phi+\cos 2\phi)$$
$$-b_1[\eta\sin 4\phi+(1+\eta)\sin 2\phi]\}, \tag{B1}$$

$$\chi_s=-\frac{1}{\pi}b_s\cos^3\phi\,\sin\phi. \tag{B2}$$

It is evident that in the first case only the edge component $\mathbf{b}_e=(\mathbf{b}_1,\mathbf{b}_2)$ of the Burgers vector appears, whereas χ_s depends only on the screw component b_s, and, moreover, it is independent of η. This result, obtained for planar channeling, is analogous to those obtained in Ref. 11 in the case of axial channeling.

Now, it is known from the literature that MD's in zinc-blende structures are mainly of the 60° type, i.e., their Burgers vector lay in the $\langle 110\rangle$ directions inclined to the dislocation lines. This means that for configuration s there are only two possibilities given by $b_s=\pm\frac{1}{2}$. From the point of view of the dechanneling probability the two possibilities are indistinguishable since the transformation $\chi\rightarrow-\chi$ has the same effect of a 180° shift of the harmonic-oscillator initial phases, which, however, are randomly distributed. For configuration e there are four different possible combinations given by $b_1=\pm\frac{1}{2}$ and $b_2=\pm 1/\sqrt{2}$. First of all, only two of them are significant, for the same reason we have just pointed out. Let the first combination correspond to $b_1>0$ and $b_2>0$ and the second to be $b_1>0$ and $b_2<0$. It is not difficult to see that we can obtain one combination from the other by substituting ϕ with $(\pi-\phi)$, i.e., by changing ξ to $-\xi$ in the solution of the equation of motion, Eq. (17). Since the ions are uniformly distributed, ξ and $-\xi$ are equally probable and the two combinations are again indistinguishable.

Figure 17 shows the behavior of the calculated distortion functions for GaAs. It is worth bearing in mind that $\chi_s(\phi)$, whose maximum is $\chi_s^{\max}=0.052$, is fully material independent. On the other hand, the distortion function $\chi_e(\phi)$ exhibits only a weak dependence on the material through the elastic constant η. For $T_2=1$, while η varies more than 12% going from η=0.686 for GaP to η=0.772 in the case of InSb, $\chi_e(\phi)$ maintains its form and its maximum, $\chi_e^{\max}$, varies less than 6% going from 0.239 to 0.253, respectively.

From Eq. (B1) it can be seen that the magnitude of $\chi_e(\phi)$ is scaled by the factor $\cos^2\gamma$, γ being the angle between the trajectory direction and its projection on the plane perpen-

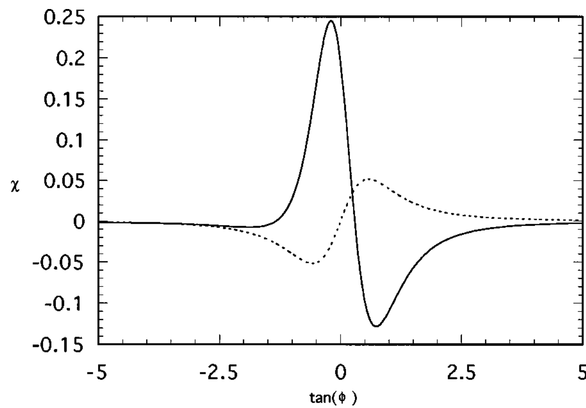

FIG. 17. The (110) planar distortion function for GaAs is reported against $\tan\phi$, which is proportional to the distance from the dislocation along the ion trajectory. The dashed and continuous lines refer to the screw and edge configuration, respectively.

dicular to the dislocation line. In this channeling configuration, the (110) plane perpendicular to the interface dislocation plane, the angle γ is simply the tilt angle between the incident beam direction and the surface normal (the [001] growth axis). Equation (B1) inserted in Eq. (A8) shows that the effect of the tilt is the same as would be obtained by reducing the density of dislocations in configuration e by a factor $\cos\gamma$. It follows that the ratio $R=P_e^{1D}/P_s^{1D}$ varies as $\cos\gamma$ and that its maximum value is given by $\gamma=0$. Actually, $\gamma=0$ corresponds to the [001] axis and experimentally it is necessary to move toward the closest planar channeling condition, which is obtained for $\gamma\approx 5°$. Since $\cos 5° \approx 1$ it is possible to drop the γ dependence in the equations. Then, for most of the semiconductors, we have $\chi_e^{max}/\chi_s^{max}>4.5$,which means that a significant difference in the dechanneling probability between configuration e and configuration s is expected.

-

*Present address: CNR-IME, Palazzo Stecca, Via Arnesano, I73100 Lecce, Italy.

[1] L. C. Feldmann, J. W. Mayer, and S. T. Picraux, *Materials Analysis by Ion Channeling* (Academic, New York, 1982).
[2] S. T. Picraux, L. R. Dawson, G. C. Osburn, R. M. Biefeld, and W. K. Chu, Appl. Phys. Lett. **43**, 1020 (1983).
[3] A. Carnera and A. V. Drigo, Nucl. Instrum. Methods Phys. Res. Sec. B **34**, 357 (1990).
[4] J. H. Van Der Merwe, J. Appl. Phys. **34**, 123 (1962); C. A. Ball and J. H. Van Der Merwe, in *Dislocations in Solids*, edited by F. R. N. Nabarro (North-Holland, Amsterdam, 1983).
[5] J. W. Matthews, S. Mader, and T. B. Light, J. Appl. Phys. **41**, 3800 (1970); J. W. Matthews and A. E. Blakeslee, J. Cryst. Growth **27**, 118 (1974).
[6] Y. Quéré, Phys. Status Solidi **30**, 713 (1968).
[7] D. Van Vliet, Phys. Status Solidi A **2**, 521 (1970).
[8] H. Kudo, J. Phys. Soc. Jpn. **40**, 1645 (1976).
[9] J. Mory and Y. Quéré, Radiat. Eff. **13**, 57 (1972).
[10] D. Wielunska, L. Wielunsky, and A. Turos, Phys. Status Solidi A **67**, 413 (1981).
[11] K. Gartner, K. Hehl, and G. Schlotzhauer, Nucl. Instrum. Methods Phys. Res. Sec. B **4**, 63 (1984).
[12] A. V. Drigo, A. Aydinli, A. Carnera, F. Genova, C. Rigo, C. Ferrari, P. Franzosi, and G. Salviati, J. Appl. Phys. **66**, 1975 (1989).
[13] M. S. Abrams, J. Blanc, and C. J. Buiocchi, Appl. Phys. Lett. **21**, 185 (1972).
[14] K. L. Kavanagh, M. A. Capano, L. W. Hobbs, J. C. Barbour, P. M. J. Marée, W. Schaff, J. W. Mayer, D. Pettit, J. M. Woodall, J. A. Stroscio, and R. M. Feenstra, J. Appl. Phys. **64**, 4843 (1988).
[15] S. Amelinckx, in *Dislocations in Solids (II)*, edited by F. R. N. Nabarro (North-Holland, Amsterdam, 1979).
[16] R. H. Dixon and P. J. Goodhew, J. Appl. Phys. **68**, 3163 (1990).
[17] V. I. Vdovin, L. A. Matveeva, G. N. Semenova, M. Ya. Skorohod, Yu. A. Tkhorik, and L. S. Khazan, Phys. Status Solidi A **92**, 379 (1985).
[18] M. Mazzer, A. V. Drigo, and F. Romanato, Nucl. Instrum. Methods Phys. Res. Sec. B **34**, 103 (1992).
[19] D. Wielunska, L. Wielunsky, and A. Turos, Phys. Status Solidi A **68**, 45 (1981).
[20] H. Kudo and M. Mannami, Phys. Lett. A **58**, 323 (1976).
[21] F. Romanato, M. Mazzer, and A. V. Drigo, Nucl. Instrum. Methods Phys. Res. Sec. B **63**, 36 (1992).
[22] H. Kudo, Phys. Rev. B **18**, 5995 (1978).
[23] K. Gartner and A. Uguzzoni, Nucl. Instrum. Methods Phys. Res. Sec. B **67**, 189 (1992).
[24] J. Lindhard, Mat. Fys. Medd. K. Dan. Vidensk. Selsk. **34**, n.14 (1965).
[25] E. Bonderup, H. Esbensen, J. U. Andersen, and E. E. Schiott, Radiat. Eff. **12**, 261 (1972).
[26] D. S. Gemmel, Rev. Mod. Phys. **46**, 129 (1974).
[27] O. H. Nielsen, F. K. Larsen, S. Damgaard, J. W. Petersen, and G. Weyer, J. Phys. Condens. Matter **52**, 99 (1983).
[28] M. Mazzer, A. Carnera, A. V. Drigo, and C. Ferrari, J. Appl. Phys. **68**, 531 (1990).
[29] L. D. Landau and E. M. Lifshitz, *Theory of Elasticity* (Pergamon, Oxford, 1986).
[30] A. Armigliato, M. Servidori, F. Cembali, R. Fabbri, R. Rosa, F. Corticelli, D. Govoni, A. Drigo, M. Mazzer, F. Romanato, S. Frabboni, R. Balboni, S. S. Iyer, and A. Guerrieri, Microsc. Microanal. Microstruct. **3**, 363 (1992).
[31] F. Romanato, A. V. Drigo, L. Francesio, P. Franzosi, L. Lazzarini, G. Salviati, M. Mazzer, M. R. Bruni, and M. G. Simeone, Microsc. Microanal. Microstruct. **6**, 491 (1995).
[32] A. A. Mbaye, D. M. Wood, and A. Zunger, Phys. Rev. B **37**, 3008 (1988).